

TED-AJ03-126

COMBINED CONDUCTIVE/RADIATIVE HEAT TRANSFER IN HIGH POROSITY FIBROUS INSULATION MATERIALS: THEORY AND EXPERIMENT

Walter W. YUEN

Department of Mechanical and Environmental Engineering
University of California at Santa Barbara
Santa Barbara, California 93106 USA
E-mail: yuen@engineering.ucsb.edu

Ezra TAKARA

Department of Meteorology
University of Maryland
College Park, Maryland 20742-2425 USA
E-mail: ezra@metosrv2.umd.edu

George CUNNINGTON

Cunnington and Associates
1958 Ivy Lane
Palo Alto, California 94303 USA
E-mail: Country33@prodigy.net

Keywords: Radiation, Conduction, LI900, Fiber, High Porosity, Zonal Method

ABSTRACT

A first-principle approach is used to analyze combined conductive/radiative heat transfer in a high porosity silica insulation materials (LI900) currently used by the Space Shuttle. Using the measured value of the refractive index (n , κ), solutions to the radiative transfer equation for fibrous insulation with a random packing geometry is used to generate macroscopic average radiative properties such as extinction coefficient, scattering albedo and phase function. Based on a non-gray application of the zonal method, transient thermal response of the insulation tile

subjected to an external radiant flux is generated and compared with experimental data. The agreement is excellent. The computation is both efficient and accurate.

Numerical results show that even with the presence of conduction and large extinction coefficient in some wavelength region, a large temperature drop ("temperature slip") occurs over a short distance near the heating surface. The inclusion of this effect is important for a correct interpretation of the heat transfer data.

NOMENCLATURE

a = absorption coefficient
 \tilde{a} = modified absorption coefficient
 A = constant in the Delta-Eddington scattering phase function
 C = specific heat
 f = forward scattering parameter
 g = anisotropic scattering factor
 $g_i g_j$ ($i, j = 1, 2, \dots, N$) = exchange factor between volume element i and j
 $(g_i g_j)^t$ ($i, j = 1, 2, \dots, N$) = total exchange factor between volume element i and j
 k = thermal conductivity
 k_{eff} = effective thermal conductivity
 k_{inf} = inferred thermal conductivity
 K_t = extinction coefficient
 \tilde{K}_t = modified extinction coefficient
 q_r = radiative flux
 $s_i g_j$ ($i = L, R, j = 1, 2, \dots, N$) = exchange factor between surface element i and volume element j
 $(s_i g_j)^t$ ($i = L, R, j = 1, 2, \dots, N$) = total exchange factor between surface element i and volume element j
 $s_i s_j$ ($i, j = L, R$) = exchange factor between surface i and surface j
 $(s_i s_j)^t$ ($i, j = L, R$) = total exchange factor between surface i and surface j
 t = time
 T = temperature

 $\delta(x)$ = the delta function
 θ = polar angle of the scattered energy
 ρ = density
 σ = Stefan Boltzmann constant
 σ_s = scattering coefficient
 $\tilde{\sigma}_s$ = modified scattering coefficient
 ϕ = azimuthal angle of the scattered energy
 Φ = scattering phase function
 $\tilde{\Phi}$ = modified scattering phase function
 ω_0 = scattering albedo
 $\tilde{\omega}_0$ = modified scattering albedo

INTRODUCTION

Heat transfer through highly porous fibrous composite materials is a problem of considerable interest because of the widespread use of fiber composites in many areas such as the development of thermal protection systems for the Space Shuttle Orbital vehicle and other commercial thermal insulation systems.

Until now, the common design practice in the insulation industry is to use the concept of "effective thermal conductivity". Using standard apparatus such as the guarded-hot-plate, data for "effective thermal conductivity" are generated. These data, together with a

conduction-only analysis package, are typically the basis of many current engineering designs for thermal insulation.

Over the past 15 years, significant advances have been made in the understanding of fundamental properties of fibrous insulation materials. There are also significant advances in both the analytical and computational capability for accurate quantitative assessment of the relevant heat transfer. Due to these advances, a first-principle approach can now be used to determine heat transfer through highly porous fibrous composite materials. In the present work, the combined conductive/radiative heat transfer through an LI900 insulation tile used by the space shuttle is generated and compared with experimental data. The agreement is excellent. The approach is also demonstrated to be computationally efficient and accurate.

For highly porous fibrous insulation materials, results show that a "temperature slip" can occur even in the presence of conduction. This phenomenon is important in the correct determination of effective thermal conductivity using conduction heat transfer apparatus such as the guarded-hot-plate.

EXPERIMENT

The experiment was conducted many years ago [1]. It is, however, still one of the few well-documented efforts available in the open literature. The data is well suited for a detailed, quantitative assessment of the computational effort.

Specifically, a quartz lamp radiant heating facility [1] was used to provide a time variant surface heat flux for the measurement of the temperature distribution in a block of the LI900 thermal insulation under a transient heating condition. The test specimen was a slab configuration 0.15 m square by 0.076 m thick. The specimen surface exposed to the radiant heat flux was coated with an opacified dense ceramic layer fusion-bonded to the insulation. Coating thickness was approximately 0.35 mm. The coating absorptance for the lamp spectrum was 0.90 and total hemispherical emittance was 0.85-0.90 over the temperature range of 300 to 1600 K. The test specimen was instrumented in the thickness direction with thermocouples located on the centerline at eight distances from the heating surface. The thermocouples were installed in a 20-mm diameter by 73-mm long cylindrical plug of the LI900 material which was press fit into a hole bored in the slab at its center. The thermocouples were made with butt-welded junctions from 0.13-mm diameter wire. The butt weld produced a 0.13-mm diameter cylinder geometry which could be accurately positioned in the specimen. Nominally, a 10-mm length of each wire extended from the butt-welded junction parallel to the slab surface so as to follow an isotherm to minimize conduction loss through the lead wires. Platinum/10-percent rhodium thermocouples were used for the two thermocouples closest to the heated surface and the remaining thermocouples were chromel-alumel. The instrumented specimen was bonded with an RTV

adhesive to a 3.18-mm thick aluminum plate. Bond layer thickness was nominally 0.13-mm. The estimated maximum uncertainty in the temperature measurement was ± 15 K. Facility calibration showed that the heat flux distribution over the surface of the test specimen was uniform to within 5 percent. A schematic of the experimental set up is shown in Figure 1.

Experiments were conducted in air at atmospheric pressure. A programmable proportional band controller was used to adjust time-dependent power to the radiant lamp bank. The control input was a thermocouple bonded in the surface coating. The radiant heating rate was automatically adjusted to follow the programmed surface temperature versus time which was to raise the surface temperature linearly from nominally 297 K to 1,533 K in 250 seconds. The temperature was then held at 1,533 K for 1,250 seconds. The radiant flux to the surface was terminated and temperature measurement continued for an additional 500 seconds of cooling. The surface temperature dropped essentially in a linear fashion to the ambient temperature (295 K) in 250 seconds. Temperature near the heating surface dropped to 550 to 600 K at the end of the measurement period. Data for one specific test using type 4.0B fibers (4 μ m diameters) which are randomly oriented in space are shown in Figure 2. These data will be used as the basis of the comparison with the computational result.

ANALYSIS

The geometry and associated coordinate system are also shown in Figure 1. The slab is assumed to be one-dimensional and the back of the aluminum substrate is subjected to a convective heat transfer coefficient h . Natural convection is neglected. Heat transfer by combined radiation and conduction are assumed for the LI900 thermal insulation while only conduction heat transfer is expected to occur in the aluminum substrate.

Radiative Heat Transfer

To determine the radiative heat transfer through the fibrous insulation, Mie theory, together with measured index of refraction (n , κ) of silica fiber, is used to generate the average extinction coefficient, absorption coefficient and anisotropic scattering factor for the insulation [2]. Assuming that fibers are packed randomly, results are shown in Figures 3 and 4. The anisotropic scattering factor, g , is an average parameter used to characterize the directional dependence of the scattering phase function. It is defined by

$$g = \frac{1}{4\pi} \int_0^{2\pi} \int_0^\pi \Phi(\theta, \phi) \cos \theta \sin \theta d\theta d\phi \quad (1)$$

where $\Phi(\theta, \phi)$ is the scattering phase function. θ and ϕ are the polar angle and azimuthal angle of the scattered energy ray relative to the incoming energy ray. It is important to note that all radiative properties depend strongly on wavelength. The material can be optically

thick in some wavelength regions and optically thin in another. The scattering effect is also significant and is highly anisotropic.

The zonal method [3] is used to determine the radiative heat flux needed for the consideration of energy conservation. The method has been demonstrated to be applicable to determine radiative heat flux and its divergence in participating media with anisotropic scattering. Due to the highly forward scattering phase function as shown by the value of g (Fig. 4), the scattering phase function is assumed to be given by the following Delta-Eddington approximation

$$\Phi(\theta, \phi) = 2f\delta(1 - \cos \theta) + (1 - f)(1 + A \cos \theta) \quad (2)$$

where $\delta(x)$ is the delta function. Substituting Eq. (2) into Eq. (1) yields the following relation between f and g

$$g = f + \frac{A(1-f)}{3} \quad (3)$$

Following the reformulation approach developed by Joseph and Wiscombe [4], the forward scattering as represented by the d -function peak can be treated not as a true extinction event since the radiation continues to propagate in the forward direction as if it has not been attenuated. This effect can be simulated by reducing the scattering coefficient to a lower value. The extinction coefficient, scattering albedo and phase function are similarly modified. Specifically, the modified properties are

$$\begin{aligned} \tilde{\sigma}_s &= (1 - f)\sigma_s \\ \tilde{K}_t &= a + \tilde{\sigma}_s = a + (1 - f)\sigma_s \\ \tilde{\omega}_0 &= \frac{\tilde{\sigma}_s}{\tilde{K}_t} = \frac{(1 - f)\sigma_s}{a + (1 - f)\sigma_s} \\ \tilde{\Phi} &= 1 + A \cos \theta \end{aligned} \quad (4)$$

The parameter A is nominally taken to be 1. Equation (3) becomes

$$f = \frac{3g - 1}{2} \quad (5)$$

The modified properties for the LI900 insulation is shown is shown in Fig. 5.

The basis of the zonal method is the computation of the total exchange factor (including the effect of scattering) between discretized zones as shown in Fig. 1. Specifically, $g_i g_j$ ($i, j = 1, 2, \dots, N$) is the exchange factor between volume element i and j . Physically, this factor is the fraction of energy leaving from element i (from both emission and scattering) which is intercepted by volume element j (after attenuation and scattering). $s_i g_i$ ($i = L, R$, $j = 1, 2, \dots, N$) is the exchange factor between surface element i and volume element j while $s_i s_j$ ($i, j = L, R$) represents the exchange factor between surface i and surface j . The physical interpretation of $s_i g_i$ and $s_i s_j$ are

similar to that of $g_i g_i$. All of these factors can be readily calculated by the Monte Carlo method. Since optical properties depend strongly on wavelength, these exchange factors are also functions of wavelength. Some specific examples, for a grid size of $dx = 0.059$ cm (128 zones in the LI900 insulation) are shown in Fig. 6a and 6b.

The exchange factors between the left wall and the adjacent zones are shown in Fig. 6a and the exchange factor between the first volume zone with the adjacent wall and the surrounding zones are shown in Figure 6b. It is important to note the strong wavelength dependence of these exchange factors. A nongray analysis is clearly necessary for the determination of radiative heat transfer. It is also important to note the relatively large value of the self-self exchange factor ($s_L s_L$, $g_i g_i$). Physically, the large scattering coefficient causes a significant fraction of the radiant energy to be re-absorbed by the surface and volume element. This is an important effect which is not captured by many of the approximation methods in radiation heat transfer (such as the multi-flux method and the diffusion method).

For energy conservation, the total exchange factors are required. They are obtained by integration over wavelength of spectral exchange factors such as those shown in Figs. 6a and 6b. The total exchange factors from the left wall to the surrounding zones and those from the first zone to the surrounding zones are shown in Figs. 7a and 7b. The strong wavelength dependence of the spectral exchange factor leads to a strong temperature dependence of the total exchange factor. Similar total exchange factors are calculated for every radiating zones within the fibrous composite materials.

Conservation Equations

Neglecting the effect of convection, the energy conservation equation for the fibrous insulation can be written as

$$\frac{\partial}{\partial t}(\rho CT) = \frac{\partial}{\partial x} \left(k \frac{\partial T}{\partial x} \right) - \frac{\partial q_r}{\partial x} \quad 0 \leq x \leq 7.6 \quad (6)$$

in the fibrous insulation and

$$\frac{\partial}{\partial t}(\rho CT) = \frac{\partial}{\partial x} \left(k \frac{\partial T}{\partial x} \right) \quad 7.6 \leq x \leq 7.918 \quad (7)$$

in the aluminum plate. For a particular discrete zone i , the radiative heat flux term can be written as

$$\begin{aligned} \left(\frac{\partial q_r}{\partial x} \right)_i &= (\sigma T_L^4 - \sigma T_i^4) (s_L g_i)^i \\ &+ (\sigma T_R^4 - \sigma T_i^4) (s_R g_i)^i \\ &+ \sum_{j=1}^N (\sigma T_j^4 - \sigma T_i^4) (g_j g_i)^i \end{aligned} \quad (8)$$

where $T_L = T(0)$, $T_R = T(x = 7.6)$ and $T_i = T(x_i)$. The aluminum plate is assumed to be opaque and thus does not contribute to the radiative heat flux in the fibrous insulation. For simplicity, the surface at $x = 0$ and $x = 7.6$ cm are assumed to be black surfaces.

The boundary condition at $x = 0$ is

$$T(0) = T_L(t) \quad (9)$$

where $T_L(t)$ is the temperature maintained at the left side of the LI900 insulation (as shown in Fig. 2). On the side of the aluminum plate, a convective boundary condition is taken to be

$$\left(k \frac{\partial T}{\partial x} \right)_{x=7.918} = h [T_a - T(7.918)] \quad (10)$$

At the interface between the aluminum plate and the fibrous insulation, energy conservation leads to

$$\left(k \frac{\partial T}{\partial x} - q_r \right)_{x=7.6-} = \left(k \frac{\partial T}{\partial x} \right)_{x=7.6+} \quad (11)$$

with the radiant heat flux at the interface given by

$$\begin{aligned} (q_r)_{x=7.6-} &= (\sigma T_L^4 - \sigma T_R^4) s_L s_R \\ &+ \sum_{i=1}^N (\sigma T_i^4 - \sigma T_R^4) g_i s_R \end{aligned} \quad (12)$$

For simplicity, no contact resistance is assumed to exist at the interface between the insulation and the aluminum plate.

Equations (6) to (12), together with the evaluation of the exchange factor and the boundary conditions, constitute a complete mathematical description of the heat transfer problem.

RESULTS AND DISCUSSION

The thermal properties of LI900 tiles were measured extensively [1,5]. In general, properties depend strongly on temperature and since the experiment is conducted in air at atmospheric pressure, the thermal conductivity must be determined experimentally, including the contribution from both the silica fiber and air. Measured values of cp and thermal conductivity, k , for the LI900 insulation is shown in Figs. 8 and 9.

Because of the lack of an effective radiation model at the time of the experiment, efforts were also made to measure the effective conductivity (including the effect of radiation) of the insulation. Two approaches were used. One approach is to simply use the guarded hot plate and determine the effective conductivity (k_{eff}) based on the total heat transfer [1]. Another approach is to conduct transient heat transfer experiment and determine an "inferred" conductivity (k_{inf}) by a nonlinear least squares

technique [6]. These data, together with the thermal conductivity data, are presented in Figure 10. The importance of radiation is quite apparent. It is interesting to note the difference in the value of the two “measured” conductivity. This illustrates the inherent uncertainty of the concept of an experimentally determined effective thermal conductivity. The value can be sensitive to both the experimental conditions and the data reduction technique.

Numerical results show that the computation converges rapidly. A grid size of $dx = 0.06$ cm (128 zones) in the fibrous insulation and a grid size of $dx = 0.053$ cm (6 nodes) in the aluminum plate is sufficient to generate converged result. For simplicity, the back of the aluminum plate is assumed to be insulated ($h = 0$). Numerical experiments show that the effect of heat transfer from the aluminum plate on the overall thermal behavior is negligible.

The predicted transient thermal behavior of the LI900 insulation is shown in Figs. 11a and 11b. Comparison between predicted and measured temperature at the eight thermocouple locations are shown in Figs. 12a to 12h. The agreement is excellent. For comparison, the “predicted” temperature using a conduction-only analysis with k_{eff} and k_{inf} are also shown in the same set of figures. The agreement is excellent, particularly in the region near the heating surface. It is important to note that for thermocouples in an environment with strong radiation, there is always a question about how the thermocouple temperature relates to the true temperature of the medium because of the difference in optical properties between the thermocouple material and the silica fiber. The thermocouple is not bonded to the fibers. It is simply in mechanical contact which can be quite poor in the case of low density fibrous media. Some uncertainty of the temperature measurement are thus expected (it is, however, difficult to estimate).

Finally, the transient temperature behavior of the three nodes within 2 mm of the heating surface is plotted on Figure 13. It is interesting to note that a temperature change as much as 100 K can occur over this short distance. This result suggests that even the fibrous material can be considered as “optically thick” from the perspective of the extinction coefficient (see Figs. 3 and 5), a “temperature slip” can occur due to the high porosity of the material and high scattering coefficient. A temperature difference of 100 K over a distance of less than 2 mm can have a significant effect, for example, on the determination of effective thermal conductivity using guarded-hot-plate data. This effect will be investigated in more detail in future works.

CONCLUDING REMARKS

A first-principle approach is demonstrated to be effective in predicting the thermal performance of LI900 composite, a highly porous fibrous insulation material. Using measured optical properties (n , κ), Mie theory and the zonal method, the transient temperature behavior of the LI900 fibrous insulation is predicted and compared

well with measurement. This approach eliminates the need to determine empirical effective thermal conductivity in the utilization of these materials for engineering systems.

Numerical results also indicate that the “temperature slip” effect, usually considered important only in radiative heat transfer in optically thin media, can occur in a highly porous fibrous insulation material. The inclusion of this effect is important in the interpretation of heat transfer data.

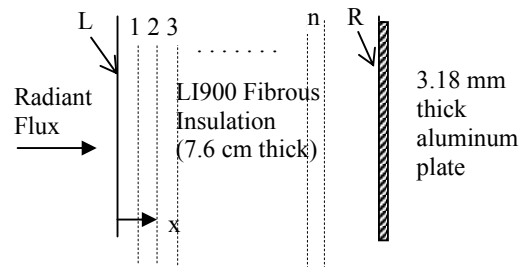


Figure 1: Experimental setup and coordinate system, the broken lines represent zonal elements used in the zonal method calculation. The numbers represent the identification of the zonal element. L and R are identification of the wall at $x = 0$ and $x = 7.6$ cm respectively.

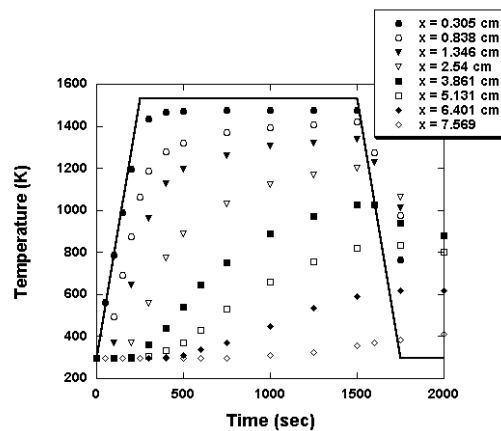


Figure 2: Transient temperature response of an LI900 tile made using Type 4.0B fibrils. (The solid line is the temperature imposed on the boundary $x = 0$ by the incident radiant flux.)

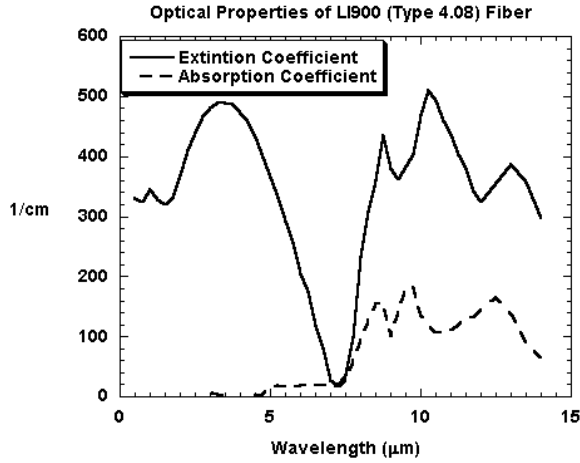


Figure 3: Computed extinction and absorption coefficient for LI900 fiber.

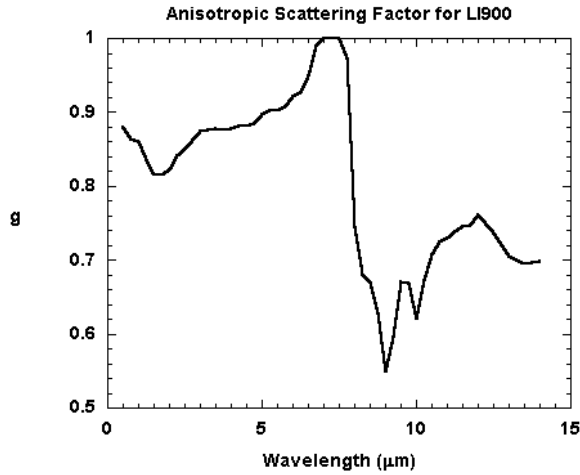


Figure 4: Computed anisotropic scattering factor for the LI900 fiber insulation.

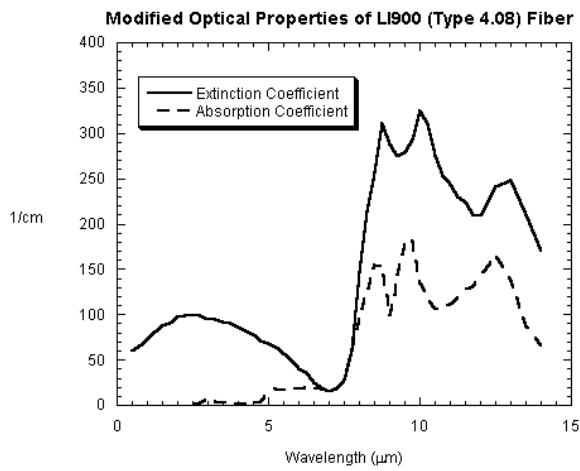


Figure 5: Modified optical properties for the LI900 fiber insulation.

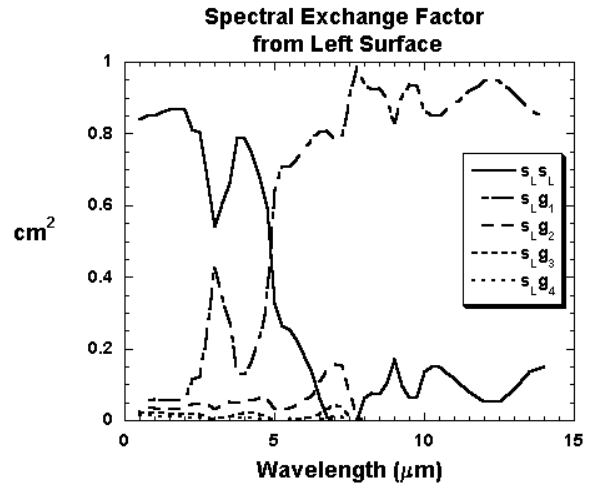


Figure 6a: Spectral exchange factor from the left surface to the surrounding zones.

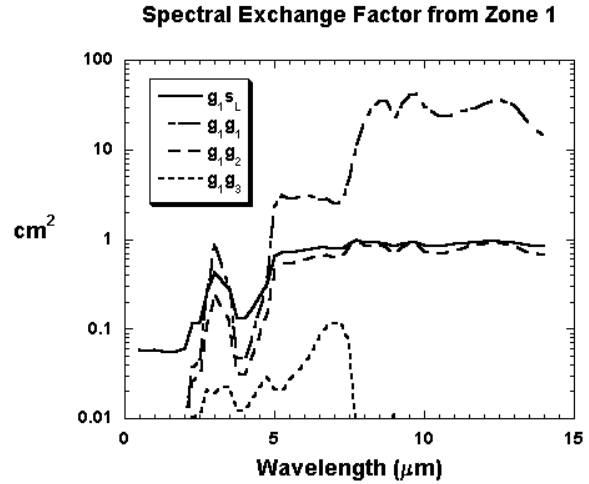


Figure 6b: Spectral exchange factor from zone 1 to the surrounding zones.

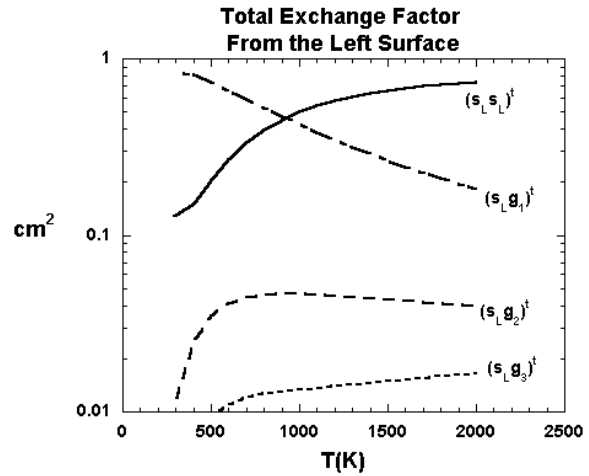


Figure 7a: Total exchange factor from the left wall to the surrounding zones.

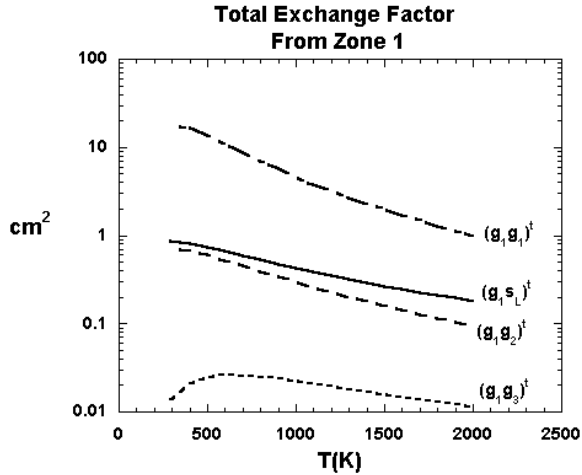


Figure 7b: Total exchange factor between zone 1 and the surrounding zones.

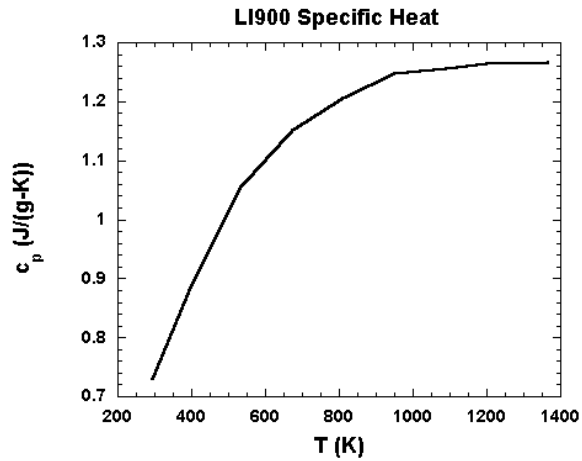


Figure 8: Measured specific heat for the LI900 Insulation.

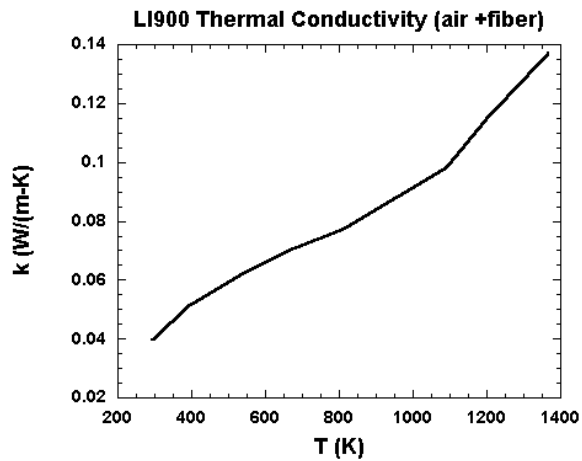


Figure 9: Measured thermal conductivity of LI900 Insulation in Air under Atmospheric Condition.

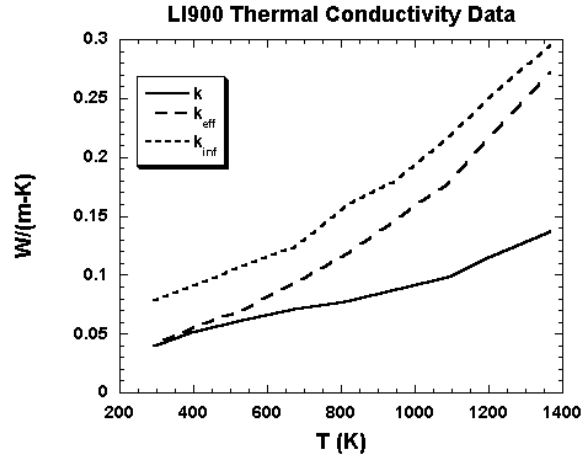


Figure 10: Comparison between the effective thermal conductivity (k_{eff}), inferred thermal conductivity (k_{inf}) and the actual thermal conductivity of the LI900 Insulation.

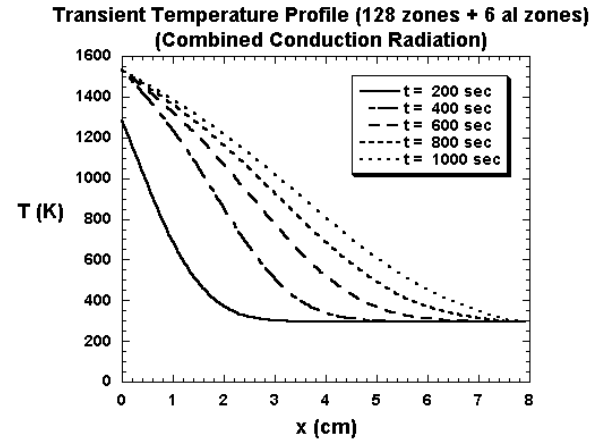


Figure 11a: Transient temperature behavior of the LI900 insulation plus aluminum plate up to 1000 sec.

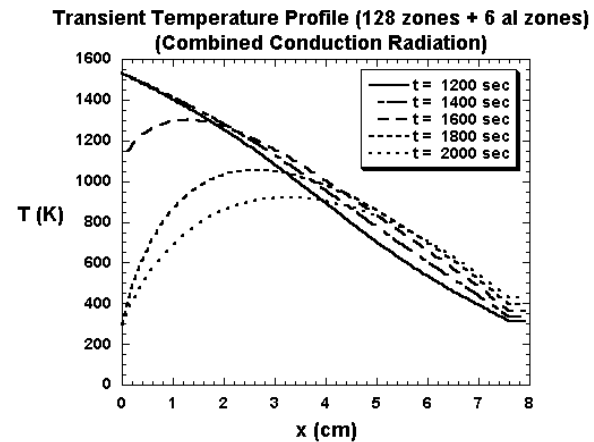


Figure 11b: Transient temperature behavior of the LI900 insulation plus aluminum plate from 1200 sec. To 2000 sec.

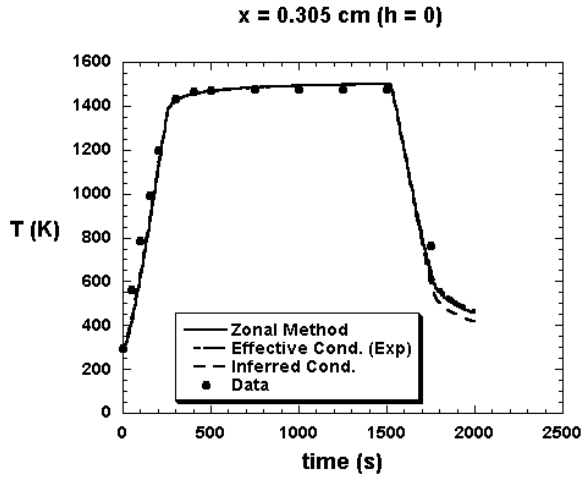


Figure 12a: Comparison between predicted and measured temperature at $x = 0.305$ cm.

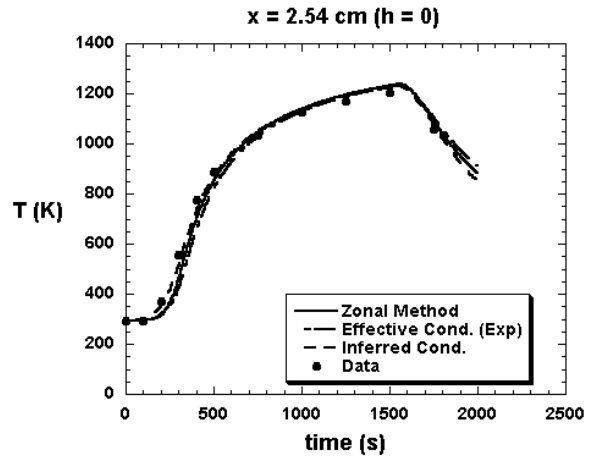


Figure 12d: Comparison between predicted and measured temperature at $x = 2.54$ cm.

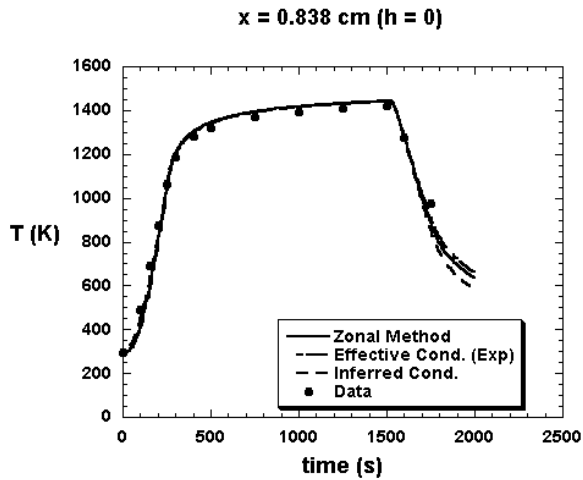


Figure 12b: Comparison between predicted and measured temperature at $x = 0.838$ cm.

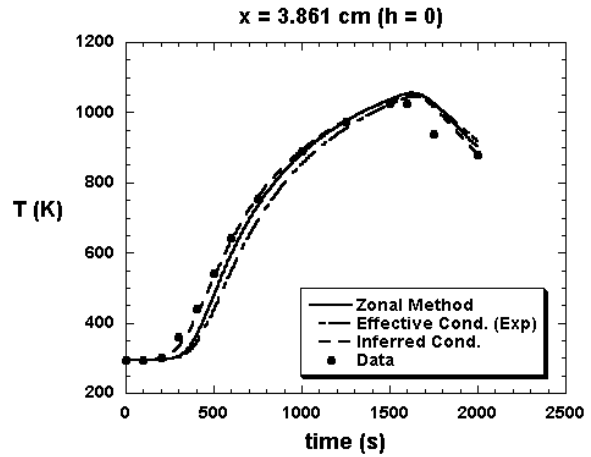


Figure 12e: Comparison between predicted and measured temperature at $x = 3.861$ cm.

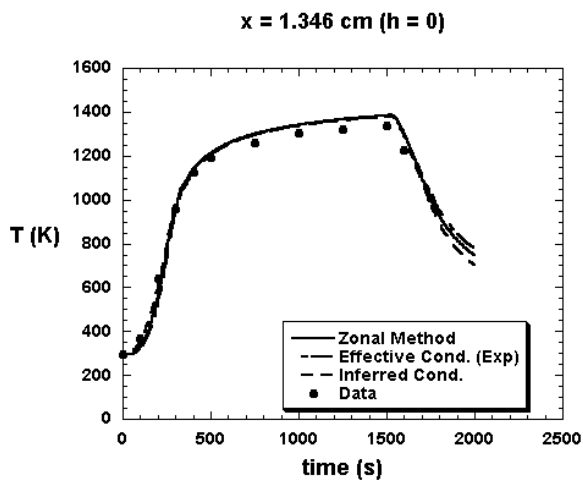


Figure 12c: Comparison between predicted and measured temperature at 1.346 cm.

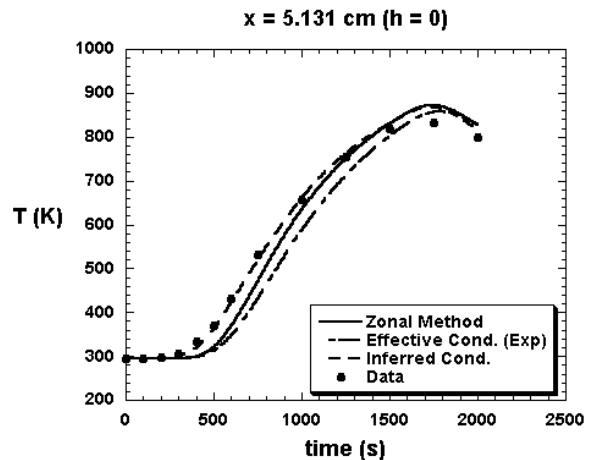


Figure 12f: Comparison between predicted and measured temperature at $x = 5.131$ cm.

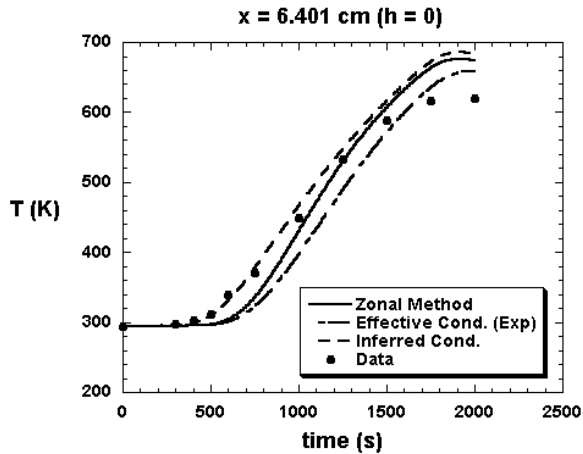


Figure 12g: Comparison between predicted and measured temperature at $x = 6.401$ cm.

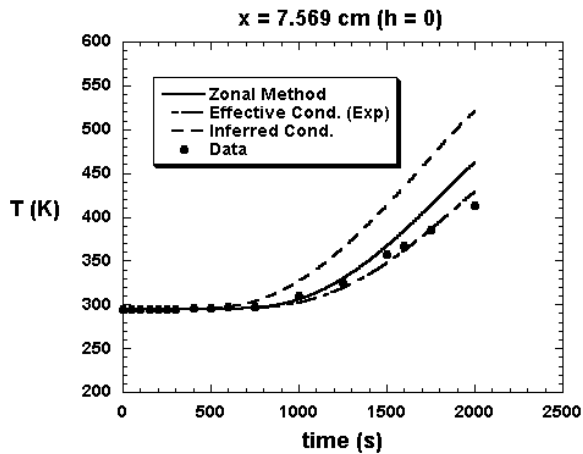


Figure 12h: Comparison between predicted and measured temperature at $x = 7.569$ cm.

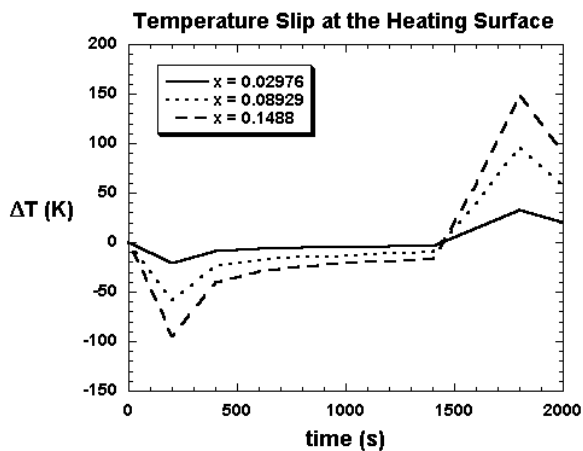


Figure 13: Temperature slip behavior at the heating surface.

REFERENCES

[1] Banas, R. P. and Cunnington, G. R., "Determination of the Effective Thermal Conductivity of the Space

Shuttle Orbiter's Reusable Surface Insulation (RSI)", AIAA Paper 74-730, 1974.

- [2] Cunnington, G. R., and Lee, S. C., "Radiative Properties of Fibrous Thermal Insulations: Theory Versus Experiment", *Journal of Thermophysics and Heat Transfer*, Vol. 10 (1996), No. 3, pp. 460-466.
- [3] Yuen, W. W. and Takara, E. E., "The Zonal Method: A Practical Solution Method for Radiative Transfer in Nonisothermal Inhomogeneous Media", *Annual Review of Heat Transfer*, Vol. 8 (1997), pp. 153-215.
- [4] Joseph, J. H., Wjiscombe, W. J. and Weinman, J. A., "The Delta-Eddington Approximation for Radiative Heat Transfer", *J. Atmos. Sci.*, Vol. 33 (1976), No. 12, pp. 2452-2459.
- [5] Data Sheet, "LI-900:Lockheed's All-Silica Insulation Materials, a Product of Space-Age Technology", Lockheed Missiles and Space Co., Inc.
- [6] Williams, S. D. and Curry, D. M., "Effective Thermal Conductivity Determination for Low Density Insulation Materials", NASA TP 1155, 1978.